Parity-Resolved State-to-State Cross Sections for Inelastic Scattering of NO $X\ ^2\Pi_{1/2}$ ($v = 20$, $J = 0.5$, *e*/*f*) from He: A Comparison between Crossed Molecular Beams Experiments and ab Initio Theory

Marcel Drabbels[†] and Alec M. Wodtke*

Department of Chemistry, University of California, Santa Barbara, California 93106

Moonbong Yang and Millard H. Alexander

Department of Chemistry and Biochemistry, University of Maryland, College Park, Maryland 20742-2021

Received: November 25, 1996; In Final Form: February 13, 1997[⊗]

Relative state-to-state cross sections for inelastic collisions between NO $X\ ^2\Pi_{1/2}$ ($v = 20$, $J = 0.5$, *e* or *f*) and He have been determined in a crossed molecular beam setup at a collision energy of 195 cm^{-1}. Efficient initial state preparation of the NO molecules is achieved by stimulated emission pumping by way of the NO $B\ ^2\Pi_{1/2}$ ($v = 5$) state. The rotational state distribution of the inelastically scattered NO molecules is probed by laser induced fluorescence through the $A\ ^2\Sigma^+(v = 3)$ state. The measured cross sections are compared with close-coupled quantum scattering calculations on both a recently reported ab initio potential energy surface (PES) and an extension of this PES which takes into account the elongation of the NO bond in $v = 20$. In the latter calculations, the highly vibrationally excited molecule is treated as a rigid rotor with a bond length equal to the average of the $v = 20$ level. Even with such an apparently drastic assumption, agreement between the experimental results and the scattering calculations on the latter PES is excellent.

I. Introduction

The pursuit of chemically accurate potential energy surfaces (PESs) has remained a long-standing objective of research in the field of molecular dynamics. Comparisons of ab initio PES and quantum scattering calculations with crossed molecular beam scattering experiments have provided one of the clearest guides to achieving this goal over the years. See for example the classic work on the reactive scattering of $F + H_2$ in ref 1 and references therein. Up to now, little work of this kind has been done with highly vibrationally excited molecules. Such highly excited molecules are known to be present in many chemical contexts, including the upper atmosphere and combustion. They may exhibit unique interactions due to their extended geometry and due to mixing with excited electronic states induced by their wild variations of bond lengths.[2] The methodology needed to treat such problems, both experimental as well as theoretical, is still in its infancy. In this paper we concern ourselves with the investigation of the interaction potential between an open-shelled highly vibrationally excited diatomic molecule, NO $X\ ^2\Pi_{1/2}$ ($v = 20$) with a rare-gas (RG) atom, He. This study provides a benchmark in the development of information regarding the interactions of highly excited molecules.

Collisional energy transfer involving radicals has been the subject of many experimental and theoretical studies. In particular, an overwhelming amount of experimental data is available for radicals in $^2\Pi$ electronic states,[3,4] which is complemented by a well-established theoretical framework.[5−10]

Because the NO radical is the only stable molecule with a $^2\Pi$ ground state, this molecule has become the paradigm of both experimental[11−30] as well as theoretical[6,7,9,31−34] studies. The first crossed molecular beam studies of collisions of NO with RGs were performed nearly 20 years ago. Keil et al.[11] measured differential scattering cross sections for collisions with He atoms while Thuis et al.[12,13] determined total scattering cross sections for state-selected NO. The results of these studies yielded considerable insight into the anisotropy of the NO−RG potential energy surfaces (PESs). The phenomenological PESs for the NO−Ar system agreed well, overall, with the PES calculated by Nielson et al.[31] using an electron gas model.

The anisotropy of the NO(X)−Ar interaction was measured in a more direct way by Andresen and co-workers,[17,20] who determined relative state-to-state integral inelastic cross sections in a crossed molecular beam apparatus. They observed a ΔJ = even propensity for scattering out of the $J = 0.5$ level. This propensity was reproduced by coupled states[32,35,36] (CS) scattering calculations based on the original and modified[17,20] versions of the electron gas PES of Nielson et al.[31] Recently, even more detailed information on NO + RG systems has been obtained from the measurement of state-to-state differential cross sections. For collisions of NO with Ar, in crossed molecular beam experiments Jons et al.[21,30] used angle-resolved, state-specific product detection, whereas Houston and co-workers[22,37] used ion imaging. For collisions of NO with He, Meyer[25] used the ion time-of-flight technique in a counterpropagating beam setup.

Concurrently, Alexander and co-workers[33,34] reported close-coupled[5,8] (CC) scattering calculations on ab initio PESs for the NO−Ar and NO−He systems, determined within the correlated electron pair (CEPA) approximation.[38−40] The calculated cross sections reproduced all of the experimentally observed features, including the rotational rainbows. Last year van Leuken et al.[26] reported parity-resolved state-to-state cross sections for scattering out of the $J = 0.5$ *f* symmetry (negative parity)[41,42] level of NO($X\ ^2\Pi_{1/2}$) in collisions with Ar. The initial state preparation was realized in this experiment via hexapole state selection. Van Leuken et al. observed strong ΔJ = even propensities for *e*/*f*[41] conserving transitions and ΔJ = odd propensities for *e*/*f* changing collisions, as had been predicted

[†] Present address: FOM Institute for Atomic and Molecular Physics, Kruislaan 407, 1098 SJ Amsterdam, The Netherlands.

[⊗] Abstract published in *Advance ACS Abstracts,* July 15, 1997.

S1089-5639(96)03898-4 CCC: $14.00

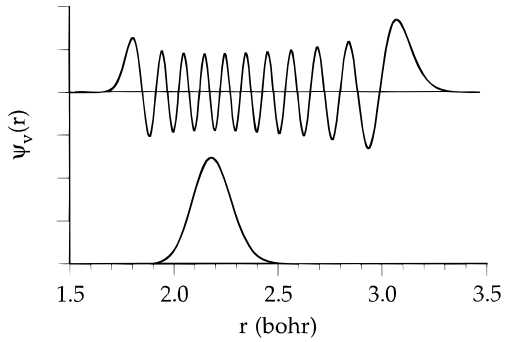

Figure 1. Plots of the vibrational wavefunctions for $v = 0$ and $v = 20$ of the $X\ ^2\Pi$ state of NO. The average values of r in the two states are $\langle r\rangle_0 = 2.183$ bohr and $\langle r\rangle_{20} = 2.604$ bohr. The minimum in the RKR potential occurs at $r_e = 2.1744$ bohr.

in the earlier scattering calculations of Alexander.[33] Very recently the same group has observed steric effects in the inelastic scattering of NO with Ar.[29] They attributed the residual discrepancies between the experimental results and those obtained by scattering calculations to errors in the PES.

All of these crossed molecular beam studies involved NO in its ground vibrational state. However, in cell experiments state-to-state rate constants have been determined for rotationally inelastic relaxation of vibrationally excited NO. Two approaches have been used to prepare the vibrationally excited molecule: IR pumping has been used to prepare molecules with a low degree of vibrational excitation ($v = 1$ or 2).[14−16,28] With these techniques, state-to-state rotational relaxation rates over a wide temperature range have been determined for collisions of NO $X\ ^2\Pi$ with He, Ar, and NO.[15,16,28] The results of the NO + RG systems at low vibrational excitation agreed perfectly with the theoretical calculations. Alternatively to IR pumping, the stimulated emission pumping (SEP) technique[43] has been used to prepare NO in highly excited vibrational states ($v \gg 1$) for use in rotational and vibrational relaxation rate experiments.[23,24,44,45]

The use of SEP for state preparation in crossed molecular beam experiments has been limited. Only very recently Ma et al.[46] performed the first study of this kind. They used SEP to prepare $I_2\ X\ ^1\Sigma_g^+$ ($v = 5$) in a molecular beam and studied the subsequent vibrational relaxation. A year later, in 1992, Bergmann and co-workers[47] used stimulated Raman with rapid adiabatic passage (STIRAP),[48] a technique very closely related to SEP, to prepare vibrationally excited Na_2, in a crossed molecular beam study of the chemical reaction of these Na_2 dimers with Cl atoms. And recently Drabbels and Wodtke[49] employed SEP in a molecular beam experiment to determine the IR Einstein *A* coefficients for highly vibrationally excited NO molecules.

In the present experiment we use SEP in combination with crossed molecular beams to study rotational relaxation in collisions of highly vibrationally excited NO molecules with He atoms under single-collision conditions. The use of SEP enables us to prepare the molecules in a unique rotational *and* Λ-doublet (parity) state. In contrast to the experiments of van Leuken et al.[26,29] where only the − parity state could be selected, we are able to prepare the NO molecules in either of the two possible parity states. Combined with parity resolved detection of the final rotational states, this provides the maximum degree of state resolution. Consequently, the observed NO−He cross sections provide the most rigorous test of the calculated NO−He interaction potential.

As shown in Figure 1, the vibrational wave function for $v = 20$, studied in this work, samples a far greater range of NO bond lengths than does the wave function of $v = 0$. This requires an improved theoretical approach. In previous calculation of the NO−He PESs[34] the NO bond was held fixed at r_e for the $X\ ^2\Pi$ state ($r = 2.1746$ bohr). The rotationally inelastic scattering cross sections computed from this surface gave good agreement with recent experiments. We describe here a new PES, in which the NO bond has been held fixed, but this time at $\langle r\rangle_{20} = 2.6037$ bohr, the average bond length of the NO bond in $v = 20$. Cross sections calculated with both this and the previous PES will be compared with the experimental results.

II. Experimental Section

A schematic overview of the experimental setup is given in Figure 2. A primary molecular beam is formed by expanding 3 atm of neat NO into a vacuum chamber through the 0.8 mm diameter orifice of a pulsed valve (General Valve) and passing it through a conical skimmer with a diameter of 2.5 mm placed 2 cm downstream of the nozzle. The pulsed valve is operated at 10 Hz and has a pulse length of 250 μs full width. The vacuum chamber is equipped with a 6 in. diffusion pump with a pumping speed of 2000 L/s. The base pressure in the chamber is 5×10^{-7} Torr and rises to 1×10^{-5} Torr with the primary molecular beam running.

Highly vibrationally excited NO molecules are produced by means of stimulated emission pumping. The NO molecules are first excited 6 cm downstream of the nozzle from the $X\ ^2\Pi$ ($v = 0$) ground state to the $B\ ^2\Pi$ ($v = 5$) valence state with the PUMP laser. They are subsequently deexcited by the DUMP laser to produce molecules in single quantum states of $X\ ^2\Pi$ ($v = 20$). A pulse-amplified single-mode ring dye laser system was used as the PUMP laser. The output of an argon ion (Spectra Physics 171) pumped single-mode ring dye laser (Coherent CR-699) operated with rhodamine 6G was pulse amplified in a home-built three-stage amplifier chain, filled with a mixture of rhodamine 610 and rhodamine 640 dyes. This system is pumped by a frequency doubled, Q-switched, injection-seeded Nd:YAG laser (Continuum Powerlite 7010-IS) with a pulse energy of 400 mJ at 532 nm and a pulse duration of approximately 5 ns. The amplified visible radiation is frequency doubled in a KDP crystal to yield 15 mJ of UV light around 300 nm. After passing a $\lambda/2$ plate, the doubled and residual fundamental radiation are frequency summed in a 1 cm long BBO crystal to yield light near 198 nm with a pulse energy of typically 2 mJ and a Fourier transform limited bandwidth of less than 200 MHz.

An excimer (Lambda Physik EMG 200) pumped dye laser (Lambda Physik FL3002) operating on coumarin 153 dye, was used to stimulate molecules (DUMP) from the electronically excited *B* state down to the $v = 20$ level of the ground electronic state. The DUMP laser, which has an output energy of 10−20 mJ/pulse and bandwidth of 0.15 cm^{-1}, counterpropagates the PUMP laser and is fired 5 ns after the PUMP laser. Both the PUMP and the DUMP laser beams have a beam diameter of approximately 3 mm. The fluorescence from the *B* state was collected with a *F*/1.6 lens system and imaged onto a photomultiplier tube (Hamamatsu R212UH) placed at right angles to both the molecular and preparation laser beams. To reduce the scattered light from both the PUMP and DUMP laser, a UG 5 color glass filter is placed in front of the phototube. Fluorescence dip measurements can be carried out with this arrangement, to ensure periodically that the SEP procedure is effective.

The secondary beam is formed by expanding 3 atm of He through a similar pulsed valve and conical skimmer. The pressure rise in the vacuum chamber with this secondary beam

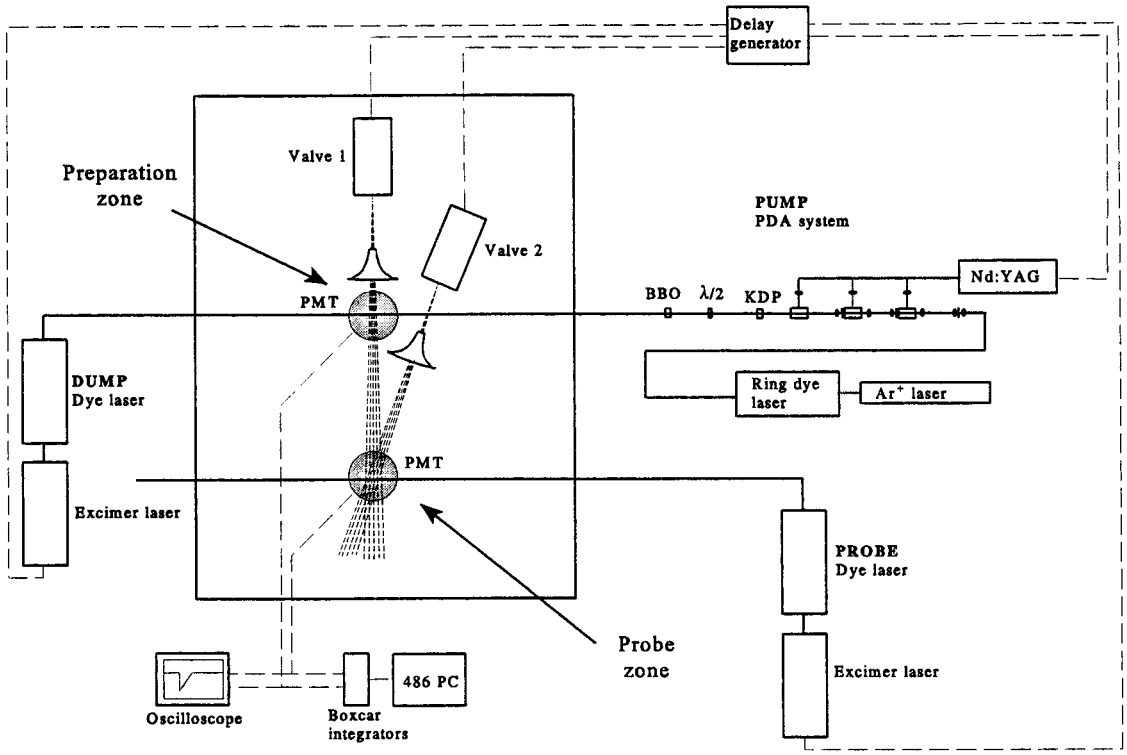

Figure 2. Schematic diagram of the crossed molecular beam arrangement. Two pulsed molecular beams are crossed in a single chamber. Stimulated emission pumping is used to prepare highly vibrationally excited NO in the primary (downward moving) beam using a pulse dye amplified laser system and an excimer-pumped dye laser. Laser-induced fluorescence is used at the crossing region of the two molecular beams to determine the state-to-state inelastic cross sections using a second excimer-pumped dye laser.

running is 5×10^{-6} Torr. The secondary beam crosses the primary beam at an angle of 30° at a distance of approximately 12.5 and 6.5 cm from the primary and secondary valves, respectively. At this crossing region a third laser beam, 5 mm beam diameter, intersects both molecular beams to PROBE the rotational distribution of the scattered NO molecules in $v = 20$. To this end a similar excimer-pumped dye laser system operating on coumarin 153 is employed which excites the molecules from the $v = 20$ level in the electronic ground state to either the $A\ ^2\Sigma^+$ ($v = 3$) state or the $B\ ^2\Pi$ ($v = 5$) state. The laser-induced fluorescence (LIF) from the electronically excited states is collected by a *F*/0.7 quartz lens system placed at right angles to both the primary molecular beam and the PROBE laser beam and imaged onto a solar blind photomultiplier tube (Hamamatsu 166UH). The signals from the photomultiplier tubes at the preparation and the collision region are both processed by a digital oscilloscope (LeCroy 9430) and boxcar integrator (SRS 250) interfaced with a 486 PC.

Just as for the NO beam, the He beam is operated at 10 Hz, but for every other shot, the opening of this valve is delayed 1 ms with respect to the primary valve. When the secondary valve is delayed 1 ms, no collisions take place between He atoms in the molecular beam and the prepared NO molecules. Thus any scattering of the initially prepared NO molecules is the result of collisions between the background gas and the NO beam or due to collisions within the NO beam. By using the boxcar integrator in "toggle mode", where the difference between every even and odd shot is integrated and averaged, the rotational energy transfer due to collisions with He can be monitored free of contributions from collisions with the background gas in the vacuum chamber.

III. Initial State Preparation

For full initial state specification, it is necessary to prepare NO molecules in a single vibrational, rotational, and parity state. Figure 3 shows a representative LIF spectrum of the band head of the $B\ ^2\Pi_{1/2}$ ($v = 5$) $\leftarrow X\ ^2\Pi_{1/2}$ ($v = 0$) system recorded at the preparation zone using the pulse-amplified ring dye laser system. The 200 MHz resolution of the laser system is clearly sufficient to resolve the two Λ-doublet components and thus to prepare a specific parity component, even for the lowest rotational levels. The output power of the PUMP laser system is high enough to saturate this transition, line broadening becomes observable at pulse energies of more than 1 mJ, so that 50% of the population in a rotational level in the ground state is transferred to the *B* state. From the observed $B\ ^2\Pi_{1/2}$ ($v = 5$) $\leftarrow X\ ^2\Pi_{1/2}$ ($v = 0$) LIF spectrum a rotational temperature of 15 K could be deduced.

Without the presence of the DUMP laser beam, the excited *B* state will radiate to various vibrational levels in the ground electronic state. The resulting vibrational distribution in the ground electronic state is determined by the Franck−Condon factors between the two electronic states, while the rotational distribution in these vibrational states is governed by the Hönl−London factors and the parity selection rule $\pm \rightarrow \mp$. The states prepared by this "Franck−Condon pumping" travel free of collisions in the molecular beam to the collision region where the rotational distribution is probed by means of LIF via the $A\ ^2\Sigma^+$ ($v = 3$) $\leftarrow X\ ^2\Pi_{1/2}$ ($v = 20$) transition. Although the Franck−Condon factor for the A ($v = 3$) $\leftarrow X$ ($v = 20$) transition is very small ($\sim 3 \times 10^{-4}$), this transition could be saturated by the unfocussed output of the PROBE laser. When probing via the A ($v = 3$) state, use can be made of the fact that for this $^2\Sigma^+ - ^2\Pi$ system the main *P*- (or *R*-) branch lines and *Q*-branch lines are well separated and probe different *e*/*f* levels of a given rotational state.[50] This allows us to resolve the final Λ-doublet state using a laser with only 0.1 cm^{-1} resolution. This should be contrasted with probing through the $B\ ^2\Pi$ ($v = 5$) state. For this $^2\Pi - ^2\Pi$ transition, the main *P*-, *Q*-, and *R*-branches occur out of both *e* and *f* levels, so that the lines appear as closely

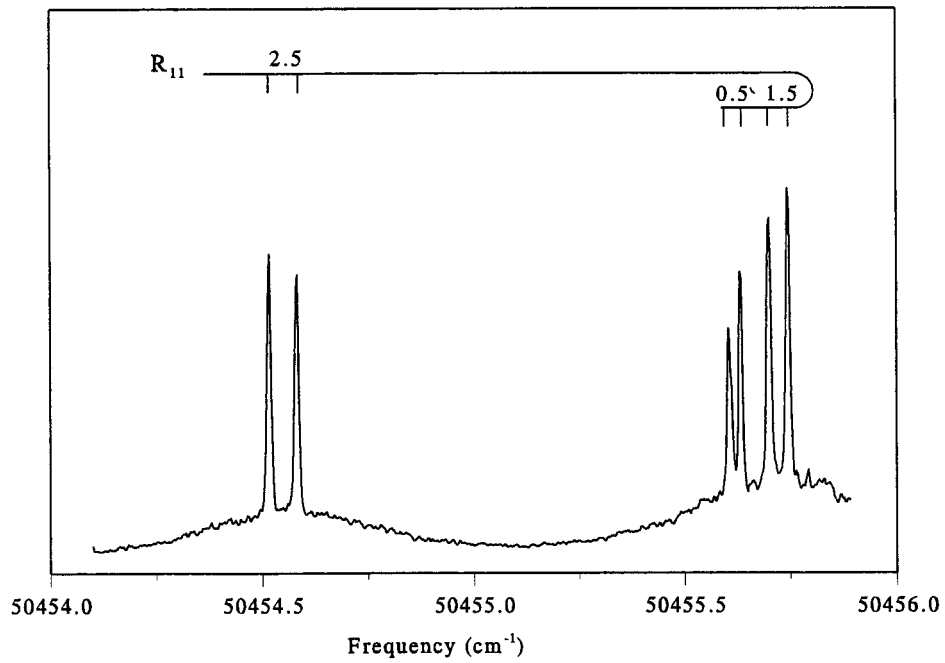

Figure 3. Representative laser induced fluorescence spectrum in the region of the NO $B\ ^2\Pi_{1/2}(v = 5) \leftarrow X\ ^2\Pi_{1/2}(v = 0)$ bandhead recorded with the pulse-amplified ring dye laser (see text). The doublet structure is due to the two Λ-doublets (*e*/*f* levels) associated with each rovibronic state.

spaced doublets.[50] Although the $B\ (v = 5) \leftarrow X\ (v = 20)$ transition has a much more favorable Franck−Condon factor (0.15), the resolution of our probe laser was too low to allow us to separate the *P*, *Q*, or *R* doublets and hence obtain information separately about the population in individual parity states of a given rotational level.

The upper panel of Figure 4 shows the LIF spectrum of the $A\ ^2\Sigma^+\ (v = 3) \leftarrow X\ ^2\Pi_{1/2}\ (v = 20)$ transition without the DUMP laser after the $B\ ^2\Pi_{1/2}\ (v = 5,\ J = 1.5,\ e)$ level has been populated. The observed population in the $v = 20$ level of the electronic ground state clearly reflects the Hönl−London factors for the $X\ ^2\Pi \leftarrow B\ ^2\Pi$ transition where both states belong to Hund's case (a):[50] strong $\Delta J = \pm 1$ and weak $\Delta J = 0$ transitions. The lower panel of Figure 4 shows the population in the $X\ (v = 20)$ level in the absence of the He beam when the DUMP laser is tuned to the $X\ ^2\Pi_{1/2}\ (v = 20,\ J = 0.5,\ e) \leftarrow B\ ^2\Pi_{1/2}\ (v = 5,\ J = 1.5,\ e)$ transition. This transition can easily be saturated which allows the enhancement of the number of molecules in the $J = 0.5$, *e*-labeled level by almost 2 orders of magnitude. Only a small fraction of the molecules are present in other rotational states. These states are populated by Franck−Condon pumping, except for the $J = 0.5$ *f* state which is most likely populated by collisions that take place in the molecular beam. Since the energy difference between the *e* and *f* states of the $J = 0.5$ rotational level is ∼300 MHz, intra-Λ-doublet transitions can take place efficiently even at very low collisional energies. We find that 95% of all the molecules in $v = 20$ are in the $J = 0.5$, *e* state. The maximum relative population in any of the other $v = 20$ rotational states is ∼1%. Since the rotational temperature in the molecular beam is 15 K and since both the PUMP and DUMP transitions are saturated, we calculate that 3% of *all* the molecules present in the beam at the preparation zone are in the prepared state, 94% are in the vibrational ground state, and 3% are in other, mainly low, vibrational states. With these numbers and the known geometry, we estimate the number density of prepared molecules in the collision zone to be 3×10^{12} molecules/cm^3.

The collision energy distribution in this experiment is determined by the velocity spreads of both molecular beams and the spread in the crossing angle between the two molecular beams. The velocity distribution of the NO beam could be determined by measuring the number of molecules in the prepared state at the collision zone as function of the time delay between the DUMP and PROBE laser. In this way, we found a mean velocity of 760 m/s with a fwhm of about 15%. This

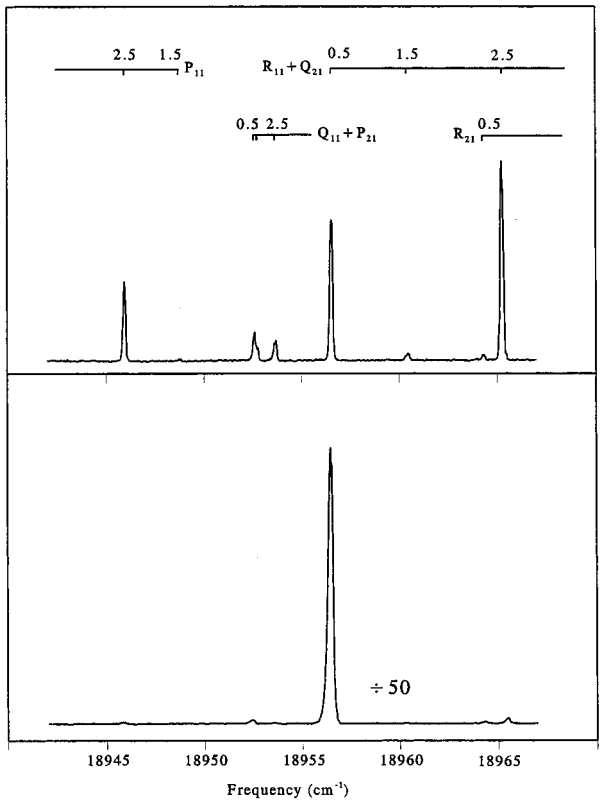

Figure 4. Preparation of single quantum states of highly vibrationally excited ($v = 20$) NO in a molecular beam. The upper panel illustrates the result of Franck−Condon pumping. The lower panel shows how SEP can be used to produce a single quantum state. We estimate that greater than 3% of the molecular beam, corresponding to a density of 3×10^{12} cm^{-3} at the collision region, is transferred to the desired state of NO $X\ ^2\Pi(v = 20,\ J = 0.5,\ e)$. The population in other nearby rotational states is almost 2 orders of magnitude lower.

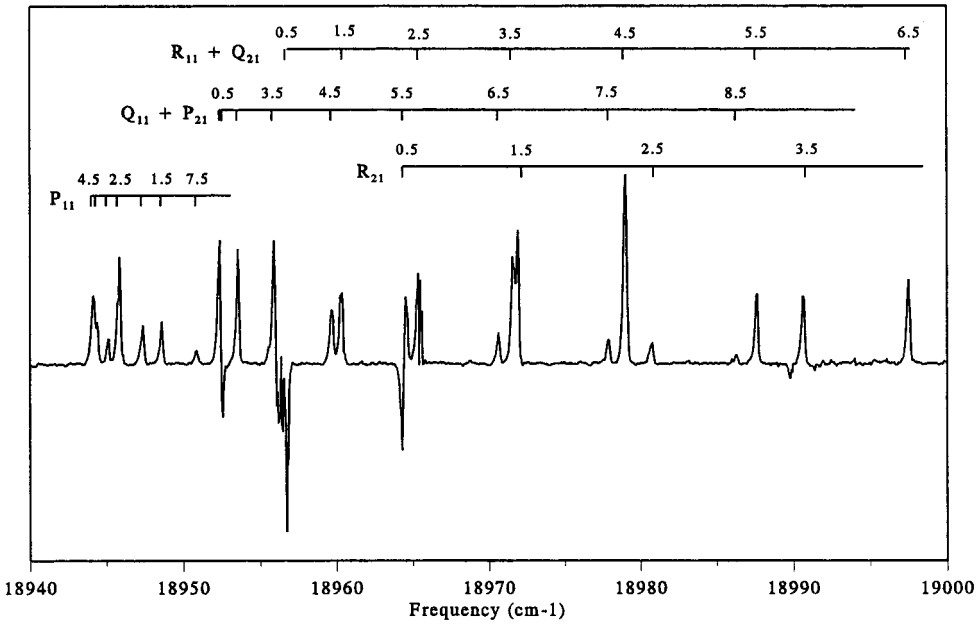

Figure 5. LIF spectrum after collision of NO $X\ ^2\Pi(v = 20, J = 0.5, e)$ with He. The negative signal (off scale) represents population removed from the prepared state(s) while the positive signals represent collisionally populated states.

value is close to that expected under conditions of adiabatic cooling in a molecular beam.[51] Using this value for the NO beam velocity and a calculated value of 1740 m/s for the He beam, we estimate that the distribution of collision energies is nearly Gaussian with a most probable collision energy of 195 cm^{-1} and a width of 65 cm^{-1} (fwhm).

IV. Experimental Observation of Inelastic Scattering

Relative state-to-state cross sections for rotationally inelastic collisions with He within the initially populated spin−orbit manifold were determined from the recorded $A\ ^2\Sigma^+$ $(v = 3) \leftarrow X\ ^2\Pi_{1/2}$ $(v = 20)$ LIF spectrum. Cross sections for collisions in which the spin−orbit state of the NO molecule was changed were found to be more than an order of magnitude weaker. These type of collisions could be probed by means of the more sensitive $B\ ^2\Pi$ $(v = 5) \leftarrow X\ ^2\Pi$ $(v = 20)$ transition which allows detection of smaller NO number densities, albeit without final-state Λ-doublet resolution. Figure 5 shows a typical $A-X$ spectrum obtained after NO molecules in the initially prepared $J = 0.5$ e level have undergone collisions with He. The spectrum is recorded using the boxcar integrator in "toggle mode". The negative signals in the spectrum therefore indicate a decrease of population (of both the prepared state as well as states populated by Franck−Condon pumping), whereas positive signals indicate an increase of population. The negative signals in this figure are not a reliable measure of the decrease of population since the detector is saturated for these transitions. The decrease of population in the prepared state due to collisions with He is hard to determine since the population fluctuations of the prepared state on the order of 20%. These population fluctuations are caused by a combination of density fluctuations in the molecular beam and beam pointing stability of the PUMP and DUMP lasers. Notwithstanding these large fluctuations, we estimate the decrease due to collisions with He to be smaller than 10%, which ensures that the experiments are performed within the single-collision regime.

From the intensities of the rotational transitions in the PROBE spectrum, we can obtain relative state-to-state cross sections. In transforming from intensities to relative cross sections, we have to take into account the following factors: (1) long-term fluctuations in the population of the prepared state, (2) the variation in line strengths in the $A-X$ band system, (3) the sensitivity to the alignment of the products, and (4) the density to flux transformation. The long-term fluctuations in the population of the prepared state are caused primarily by the frequency drift of the cw ring dye laser. Since the DUMP step is strongly saturated and no drift of this laser was observed, the $B-X$ LIF signal detected at the preparation region is proportional to the number of prepared molecules. Thus, to correct for the population drift of the prepared state, the recorded $A-X$ laser-induced fluorescence spectra that are used to determine the rotational state distribution of the scattered molecules were normalized with respect to this $B-X$ LIF signal, simultaneously recorded at the preparation zone of the machine.

Since the $A-X$ transition could be saturated by the output of the PROBE laser, it is not necessary to correct for a variation in line strengths. Thus the measured intensities are a direct measure of the densities of the states probed, once the degeneracies of the levels are taken into account. Further, saturating the transition greatly reduces the sensitivity of the LIF signal to possible alignment of the NO products. Measurements of the LIF signals on various rotational transitions with different polarizations of the probe laser, at laser powers low enough to avoid saturation, showed that no alignment effects could be detected to within experimental uncertainty. This validates the direct conversion from LIF intensities to densities.

It has been shown by McDonald and Liu[52] that when the dimensions of that part in the molecular beam containing the molecules under investigation, in their case CH radicals produced by laser photolysis and in our case NO X $(v = 20)$ produced by SEP, are smaller than the size of the probe volume, so that all products are detected regardless of their final lab velocities, fluxes are measured rather than densities. If the experiment were to measure densities rather than fluxes, a density-to-flux transformation would have to be performed. Calculations show that this correction is less than 10% for elastic transitions and even less for inelastic transitions. Since in the present experiment we are close to the regime where we measure fluxes rather than densities and the correction for the density-to-flux transformation is smaller than the experimental uncertainty, it was decided to convert the observed LIF intensities directly to fluxes.

To increase the precision of the relative cross sections, the results of 10−15 scans were averaged. Additionally, various choices of PUMP and DUMP transitions were used to prepare the initial state to eliminate any influence of Franck−Condon pumping on the derived relative cross sections.

V. Ab Initio Potential Energy Surfaces

As mentioned earlier, to describe correctly the interaction of He with NO $X\ ^2\Pi$ ($v = 20$) it is necessary to take into account the substantial elongation of the NO bond, as compared to its equilibrium value. The most complete description would involve determination of the PES for many values of the NO bond distance, which would then be averaged over the vibrational wavefunction of the molecule in $v = 20$.[53] Since the determination of the NO−He PES, even for one value of the internuclear NO distance r, is a computationally demanding endeavor, we decided to forgo this approach but instead calculate a new NO−He PES keeping the NO bond length fixed at the average internuclear distance in $v = 20$ ($r = 2.6037$ bohr). In contrast, our previous NO−He PES[34] was calculated with the r fixed at its equilibrium value ($r = 2.1746$ bohr). Except for the change in the NO bond distance, the method and the basis set used in the calculation were unchanged from our previous ab initio study of the He−NO ($X\ ^2\Pi$) PES.[34] The calculations made use of the correlated, size-consistent CEPA method,[38−40] and the recent augmented correlation-consistent valence quadruple-ζ (*avqz-f*) basis of Dunning and co-workers[54,55] with the exclusion of *g* functions on N and O and *f* functions on He (13*s*7*p*4*d*3*f* contracted to 6*s*5*p*4*d*3*f* for N and O and 7*s*4*p*3*d* contracted to 5*s*4*p*3*d* for He). All calculations were carried out with the MOLPRO suite of ab initio programs.[56]

The ground electronic state of NO ($X^2\Pi$) has a nominal electron occupancy of $...5\sigma^2 1\pi^4 2\pi^1$. As a collision partner approaches, the doubly degenerate $X\ ^2\Pi$ state will split into *two* electronic states, one of A' and one of A'' symmetry (in C_s geometry).[5,8,57−59] The symmetry reflects the orientation of the unpaired π electron with respect to the triatomic plane.

The NO−He(X) PESs are described in terms of the distance R from the center of mass of NO to the He atom, fixed NO bond length r, and the angle θ between $\vec{R}$ and $\vec{r}$. The interaction energy for each angle θ and for each electronic state (A' or A'') is defined as

$$V(R) = E_{\mathrm{He-NO}}(R) - E_{\mathrm{NO}}(\infty) - E_{\mathrm{He}}(\infty) - \Delta E_{\mathrm{CP}}(R) \quad (1a)$$

Here the counterpoise correction,[60] which adjusts for the lack of saturation of the orbital basis, is defined by

$$\Delta E_{\mathrm{CP}}(R) = E_{\mathrm{NO}}(R) + E_{\mathrm{He}}(R) - E_{\mathrm{NO}}(\infty) - E_{\mathrm{He}}(\infty) \quad (1b)$$

Since the CEPA method[38−40] is size-consistent, there is no additional correction for residual size consistency.

Ab initio calculations of the interaction energies were carried out at seven values of θ ($\theta = 0°$, 30°, 60°, 90°, 120°, 150°, 180°) and 14 values of the center-of-mass separation R (4, 4.5, 5, 5.5, 6, 6.5, 7, 7.5, 8, 8.5, 9, 10, 11, and 12 bohr). The angle $\theta = 0$ corresponds to collinear He−NO. For the A' state, at short distances ($R < 5$ bohr for $\theta = 60$ and 120° and $R < 6$ bohr for 30 and 150°) the CEPA calculations do not converge. This is due to significant mixing with next higher state of A' symmetry which corresponds to NO($A\ ^2\Sigma^+$) + He. These values of R lie high on the repulsive wall of the A' PES, considerably inside the classical turning point at the experimental collision energy of 195 cm^{-1}. Consequently, we can interpolate the PES at these points with little loss of accuracy. To do so we use the approximation

$$V_{A'}(R, \theta) = V_{A''}(R, \theta)\, V_{A'}(R, \theta{=}0)/V_{A''}(R, \theta{=}0) \quad (2)$$

with which the value of the A' PES at the points at which convergence cannot be achieved is approximated by the value of the A'' PES at the same points, multiplied by the ratio of the A' to A'' PES at collinear geometry and the same value of R.

For each value of θ the calculated $V_{A'}$ and $V_{A''}$ PESs were fit to a function of R of the general form

$$V(R) = c_1 \exp(-b_1 R) + (c_2 + c_3 R) \exp(-b_2 R) + c_4\, (\tanh[1.2(R-R_0)] - 1)/R^6 \quad (3)$$

The six parameters were adjusted to minimize the relative fit of eq 3 to the ab initio data. The rms relative error in the final fit, averaged over all values of θ, was <0.1%.

Figures 6 and 7 display contour plots of the $\langle r\rangle_{20}$ A' and A'' PESs. For comparison these are compared with similar contour plots of the r_e PESs. Although the qualitative features are similar there are some noticeable differences. First, the $\langle r\rangle_{20}$ PESs are shifted outward, particularly for linear geometries, which will result in a larger angular anisotropy. The minima in the r_e and $\langle r\rangle_{20}$ A' PESs both occur near perpendicular geometry and have the same qualitative aspect. However, the angular variation of the $\langle r\rangle_{20}$ A'' PES is considerable flatter than in the r_e A'' PES and lacks the pronounced minima at $\theta \approx 60°$ which is present in the r_e A'' PES.

In the subsequent scattering calculations, it is physically appropriate to use the average and half-difference of the $V_{A'}$ and $V_{A''}$ PESs.[8] The matrix elements of the PESs are usually expressed as sums of terms $V_{\lambda 0}(R)$ and $V_{\lambda 2}(R)$, which arise from the expansion of the θ dependence of these "sum" and "difference" PESs, namely[5,8]

$$V_{\mathrm{sum}}(R,\theta) \equiv {}^1/_2[V_{A''}(R,\theta) + V_{A'}(R,\theta)] = \sum_{\lambda=0}^{\lambda_{\max}} V_{\lambda 0}(R)\, d^{\lambda}_{00}(\theta) \quad (4a)$$

$$V_{\mathrm{dif}}(R,\theta) \equiv {}^1/_2[V_{A''}(R,\theta) - V_{A'}(R,\theta)] = \sum_{\lambda=0}^{\lambda_{\max}} V_{\lambda 2}(R)\, d^{\lambda}_{20}(\theta) \quad (4b)$$

where $d^{\lambda}_{mn}(\theta)$ is a reduced rotation matrix element. In linear geometry, the A′ and A″ states become the two degenerate components of a Π electronic state. Consequently, V_{dif} vanishes for $\theta = 0$ and 180°. Figure 2 of ref 34 illustrates the R dependence of the $V_\lambda(R)$ terms in the expansion of V_{sum} and V_{dif} for the r_e PESs. For both V_{sum} and V_{dif} the largest terms correspond to even λ (V_{20} and V_{42}). This is a manifestation of the near homonuclear character of the NO molecule.[17] As will be discussed below, the dominance of the even-λ terms leads to marked differences in the magnitudes of the calculated cross sections.

Figure 8 compares the larger $V_\lambda(R)$ terms in the expansions of the r_e and the $\langle r\rangle_{20}$ PESs. We observe that the $V_{\lambda 0}(R)$ terms are consistently larger for the latter PESs. This indicates that, averaged over both orientations of the 2π orbital, both the effective "size" of the molecule (as manifested by the V_{00} term) and the angular anisotropy (as manifested by the V_{10} and V_{20} terms) are larger when the NO molecule is highly vibrationally excited. In contrast, the difference potential, which is a manifestation of the difference in the angular anisotropy corresponding to the two orthogonal orientations of the 2π electron, is comparable in magnitude, if not slightly smaller,

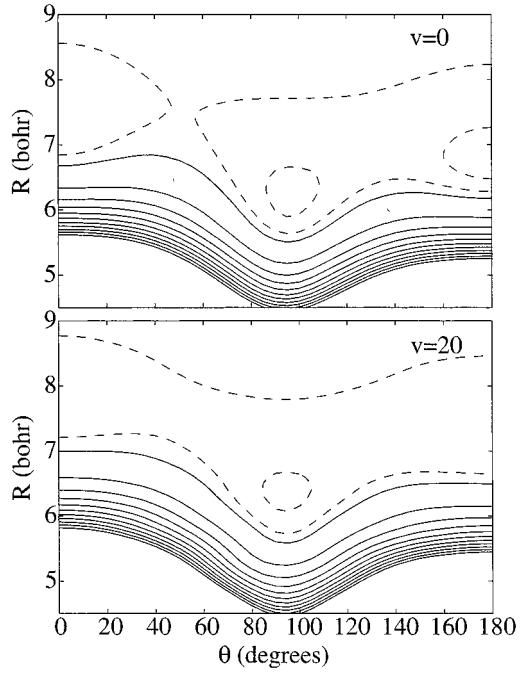

Figure 6. Contour plots of the NO(X)−He CEPA A' PESs. The upper and lower panels correspond, respectively, to the $\langle r\rangle_{20}$ and r_e PESs (see text). The collinear He−NO geometry corresponds to $\theta = 0°$. The dashed contours indicate negative energies with the first contour at -10 cm^{-1} and a spacing of 10 cm^{-1}. The solid contours designate positive energy; the contours are equally spaced with the first contour at 0 cm^{-1}, a spacing of 50 cm^{-1}, and the last (innermost) contour at 500 cm^{-1}.

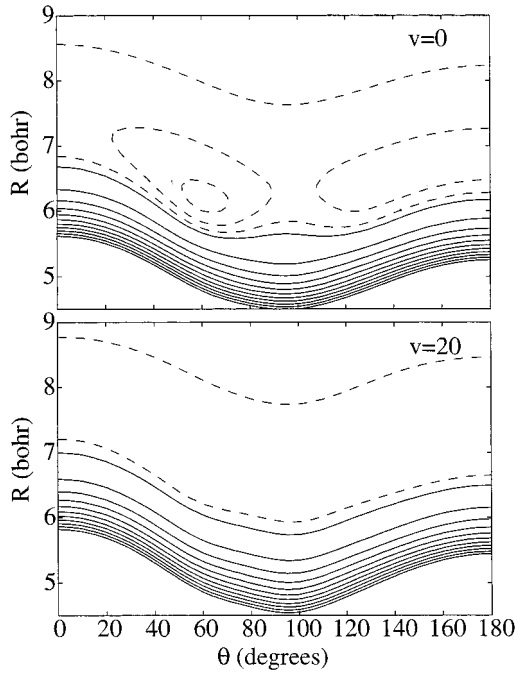

Figure 7. Contour plots of the He−NO(X) CEPA A'' PESs. The upper and lower panels correspond, respectively to the $\langle r\rangle_{20}$ and r_e PESs (see text). The collinear He-NO geometry corresponds to $\theta = 0°$. The dashed contours indicate negative energies with the first contour at -10 cm^{-1} and a spacing of 10 cm^{-1}. The solid contours designate positive energy; the contours are equally spaced with the first contour at 0 cm^{-1}, a spacing of 50 cm^{-1}, and the last (innermost) contour at 500 cm^{-1}.

when the NO molecule is highly vibrationally excited. Thus, with increasing vibrational excitation, the NO molecule in its $X\ ^2\Pi$ state becomes more anisotropic, but its open-shell character is diminished.

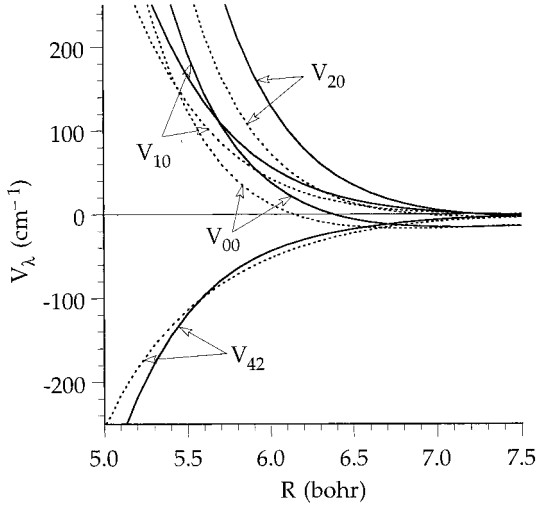

Figure 8. Plots of the R dependence of the largest $V_\lambda(R)$ terms (in cm^{-1} units) in the expansion in reduced rotation matrix elements of the NO−He $\langle r\rangle_{20}$ PESs (solid curves). These are compared with the same $V_\lambda(R)$ terms in the expansion of the r_e PESs (dashed curves). The $V_{\lambda 0}(R)$ and $V_{\lambda 2}(R)$ coefficients refer, respectively, to the sum potential (eq 4a) and the difference potential (eq 4b).

VI. Quantum Scattering Calculations

The formal theory of the scattering of a spherical atom and a $^2\Pi$ diatom has been described in detail elsewhere[5,8−10] and is not reproduced here. The wave function of the molecule is expanded in a Hund's case (*a*) basis, in which the basis functions are defined by the total angular momentum, J, with projections M and Ω along the space- and molecule-fixed z axes, respectively, and the parity index ϵ. The quantum number Ω, which can equal $^1/_2$ or $^3/_2$, is the sum of the projections of the electronic orbital (Λ) and spin (Σ) angular momenta along the molecule-fixed z axis. The *e*- and *f*-labeled Λ-doublet states[41] correspond, respectively, to $\epsilon = +1$ and $\epsilon = -1$. The total parity of the molecular rotational−electronic states is given by $\epsilon(-1)^{J-1/2}$.[41]

In the pure Hund's case (*a*) limit, where Ω is a good quantum number,[61] spin−orbit conserving transitions will be induced only by the average potential V_{sum} and spin−orbit changing transitions, only by the difference potential V_{dif}.[5] The definite-Ω states are mixed by the $(\boldsymbol{J} - \boldsymbol{L} - \boldsymbol{S})^2$ term in the molecular Hamiltonian.[50,61] Although the rotational constant of NO in $v = 20$ ($B = 1.3297$ cm^{-1})[62] is much smaller than the spin−orbit constant ($A = 114.01$ cm^{-1}),[62] only at low J is NO correctly described as a pure Hund's case (*a*) molecule. In the "intermediate coupling" regime the mixed states are labeled F_1 and F_2 (in order of increasing energy). In our calculations the electronic−rotational wave functions of the NO molecule are described in the correct intermediate coupling representation. However, since the mixing is small over the range of rotational states probed in the experiment, we will use the nominal quantum number Ω to label the states.

The collisional coupling between any pair of levels, at least one of which is described in this intermediate coupling regime, will involve both the average and difference potentials.[10] The degree of quantum interference, involving collisions which sample simultaneously both the A' and A'' PESs, will be governed by the degree of mixing of the pure Hund's case (*a*) basis states.[10,33]

At a total collision energy of 195 cm^{-1}, which is the mean energy in the experiment, we carried out close-coupling[5,63] calculations of the integral cross sections based on both the previously determined r_e PESs[34] and the new $\langle r\rangle_{20}$ PESs. The integration parameters were all adjusted to ensure convergence

of the calculated S matrix elements to an accuracy of better than 1%. The maximum values of the total NO−He angular momentum used in the calculations was 45.5. All NO electronic−rotational levels up through $J = 11.5$, the highest energetically allowed rotational level, were included. For the calculations with both the r_e and $\langle r \rangle_{20}$ PESs, the rotational and spin−orbit coupling constants appropriate to NO $X\ ^2\Pi$ ($v = 20$), $B = 1.3297$ cm^{-1} and $A = 114.01$ cm^{-1},[62] were used to determine both the internal energies of the electronic−rotational basis states (channels) and in the molecular Hamiltonian[50,61] which couples the Hund's case (*a*) states. The quantum scattering calculations were carried out with our HIBRIDON package.[64]

VII. State-to-State Cross Sections: Comparison of Experiment and Theory

In the Hund's case (*a*) limit, the two *e/f* conserving transitions ($e \rightarrow e$ and $f \rightarrow f$) will be equally probable as will the two *e/f* changing transitions ($f \rightarrow e$ and $e \rightarrow f$).[5] As we have seen in our previous studies of collisions of NO with He[34] and Ar,[33] due to the slight deviation from pure Hund's case (*a*) coupling, both the average and difference PESs will contribute to a given $J \rightarrow J'$ transition. Quantum interference can then occur, which results in preferential population of one or the other Λ-doublet level in the final rotational state. For fine-structure conserving transitions, there is a slight, but consistent, tendency to populate preferentially states which are antisymmetric, $\Pi(A'')$, f symmetry,[65] with respect to the reflection of the spatial part of the electronic wave function in the plane of rotation of the $^2\Pi$ molecule.

Experimental cross sections were obtained for scattering, separately, out of the e and f Λ-doublet levels of $J = 0.5$. Unfortunately, it is not possible to observe the quantum interference effects mentioned above since the experimental cross sections for scattering out of the two separate initial states cannot be put on the same relative scale. Since the cross sections for scattering out of the e and f levels are expected to be nearly equal for the NO−He system, both the experimental and theoretical cross sections are averaged over both initial states, in other words

$$\sigma_{\text{exp},e/f\ \text{conserving}} = {}^1/_2[\sigma_{e\rightarrow e} + \sigma_{f\rightarrow f}] \tag{5a}$$

$$\sigma_{\text{exp},e/f\ \text{changing}} = {}^1/_2[\sigma_{e\rightarrow f} + \sigma_{f\rightarrow e}] \tag{5b}$$

Further, to normalize the experimental cross sections for spin−orbit conserving transitions, we set the sum of the measured inelastic cross sections, out of the $J = 0.5$ state into all accessible rotational states in the $\Omega = 0.5$ spin−orbit manifold, equal to the calculated value for the $\langle r \rangle_{20}$ PESs.

A comparison between the experimental and theoretical cross sections, based on both the $\langle r_e \rangle$ and $\langle r \rangle_{20}$ PESs can be found in Table 1 and Figures 9 and 10. We see that the agreement between theory and experiment is excellent, both in the overall dependence of the cross sections on ΔJ and in the modulation depth of the pronounced oscillatory structure. This latter is a consequence of the near-homonuclear character of the NO molecule and has been discussed in detail in several earlier publications.[5,8,66]

From the fully quantum treatment of the scattering, one can show that the *even-λ* terms in the expansion of both the average and difference PESs will couple *e/f conserving* transitions with *even* ΔJ and *e/f changing* transitions with *odd* ΔJ. The reverse holds for the *odd-λ* terms in the expansion of the PESs. This then explains the pronounced oscillations seen in Figure 9 for the NO−He system, where *even-λ* terms dominate (see Figure 8 and Figure 2 of ref 34). In a recent study of Ar−OH($X\ ^2\Pi$) collisions, Degli-Esposti et al.[66] predicted that if the *even-λ* terms dominate the expansion of the angular dependence of the PESs, then a tendency to conserve the total parity will emerge. In a recent invetsigation of Ar−NO(X $^2\Pi$, $v = 0$)−Ar collisions,[26] both theoretical calculations and experimental state-resolved measurements uncovered a similar propensity to conserve the total parity. Because the total parity is $(-1)^{J-1/2}$ for e and $-(-1)^{J-1/2}$ for f levels,[41] this propensity is equivalent to what is

TABLE 1: Experimental and Theoretical State-to-State Cross Sections (Å^2) for Spin−Orbit Conserving ($\Omega = {}^1/_2 \rightarrow \Omega = {}^1/_2$) Transitions in Collisions of NO $X\ ^2\Pi_{1/2}$($v = 20$, $J = 0.5$, *e/f* Symmetry) with He at an Average Collision Energy of 195 cm^{-1}

		theory[b]	
J'	exp[a]	r_e PES	$\langle r \rangle_{20}$ PES
	e/f Conserving[b]		
0.5	*c*	*d*	*d*
1.5	1.47 ± 0.23	1.67	1.26
2.5	6.00 ± 0.60	5.78	6.30
3.5	1.58 ± 0.12	1.56	1.15
4.5	3.14 ± 0.37	2.03	3.83
5.5	1.02 ± 0.13	0.50	1.18
6.5	1.25 ± 0.12	0.50	0.94
7.5	0.40 ± 0.07	0.05	0.25
8.5	0.37 ± 0.07	0.04	0.09
	e/f Changing[e]		
0.5	*f*	0.85	0.63
1.5	3.75 ± 0.52	3.98	4.28
2.5	1.25 ± 0.15	1.23	0.87
3.5	2.35 ± 0.18	1.74	3.21
4.5	0.94 ± 0.08	0.47	1.05
5.5	1.21 ± 0.15	0.50	0.89
6.5	0.41 ± 0.07	0.06	0.27
7.5	0.41 ± 0.08	0.05	0.12
8.5	0.12 ± 0.03	0.01	0.01
	Total[g]		
1.5	5.22 ± 0.57	5.65	5.54
			5.59
2.5	7.25 ± 0.62	7.01	7.17
			7.20
3.5	3.93 ± 0.22	3.30	4.36
			4.32
4.5	4.08 ± 0.38	2.50	4.88
			4.83
5.5	2.23 ± 0.20	1.00	2.07
			2.06
6.5	1.66 ± 0.14	0.56	1.21
			1.20
7.5	0.81 ± 0.11	0.10	0.37
			0.37
8.5	0.49 ± 0.08	0.05	0.10
			0.12
$\langle \Delta E_{\text{rot}} \rangle$[h]	24.5 ± 0.9	16.6	21.4

[a] The absolute magnitude of the experimental cross sections is set by setting their sum equal to the sum of the calculated $\langle r \rangle_{20}$ cross sections. The reported values are given within a 95% confidence level. [b] The tabulated theoretical values are the average of the $e \rightarrow e$ and $f \rightarrow f$ cross sections (eq 5a). [c] No information on the elastic scattering could be obtained in the present experiment. [d] The scattering calculations did not extend to sufficiently large values of the total angular momentum (impact parameter) to ensure convergence of this elastic cross section. [e] The tabulated theoretical values are the average of the $e \rightarrow f$ and $f \rightarrow e$ cross sections (eq 5b). [f] No experimental information could be obtained on the intra-Λ-doublet collisions due to population of these levels by collisions in the molecular NO beam. [g] The tabulated theoretical values are the summed and averaged cross sections defined by eq 7. The second line in the fourth column corresponds to an average, over the experimental distribution of collision energies, determined using cross sections calculated at $E = 162$, 195, 228, and 300 cm^{-1}. [h] The average rotational energy transfer in cm^{-1}, defined by eq 6.

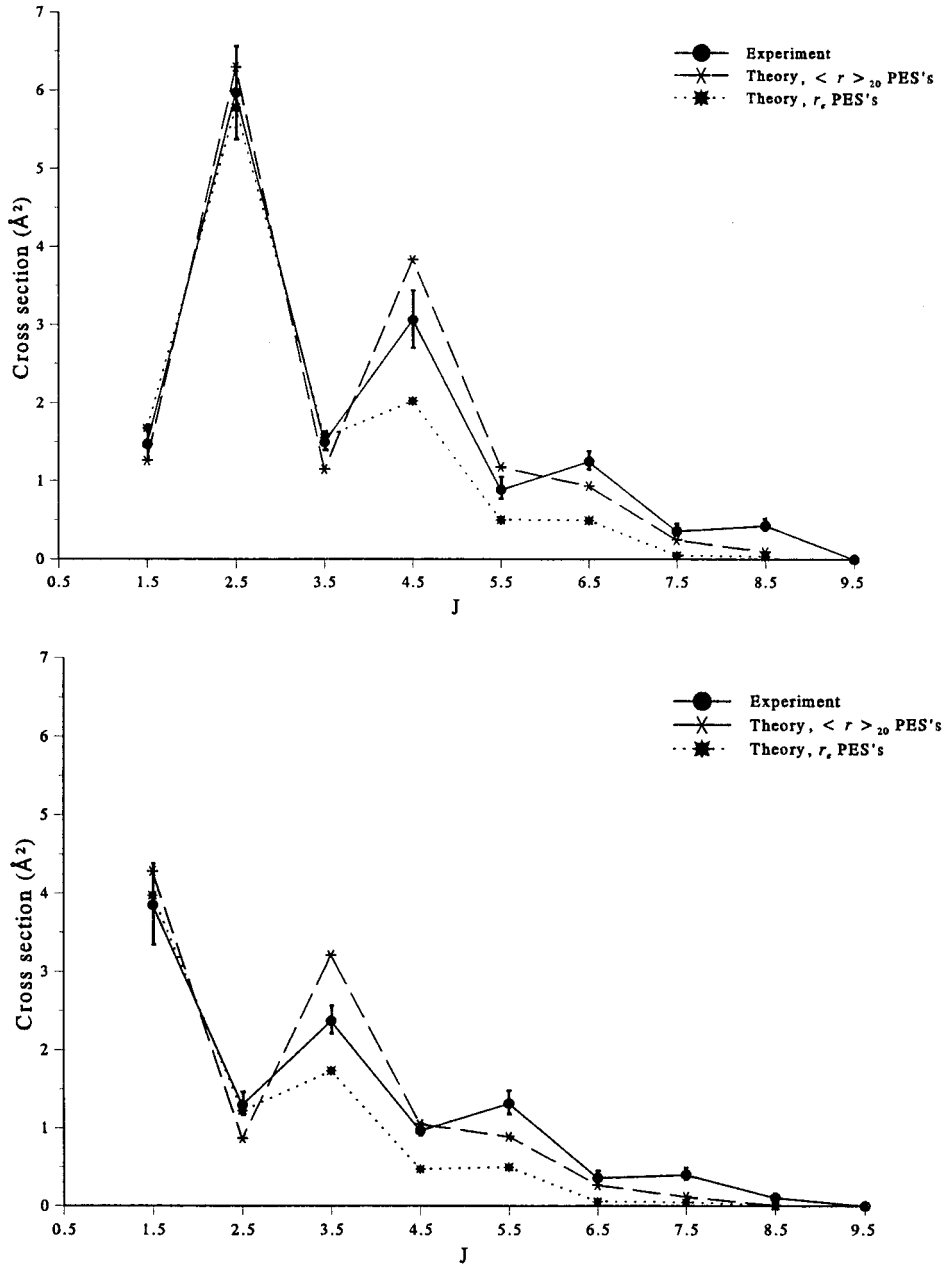

Figure 9. Comparison of the experimental and theoretical cross-sections for spin−orbit conserving ($\Omega = {}^1/_2 \rightarrow \Omega = {}^1/_2$) transitions (taken from Table 1). To guide the eye the points have been connected by straight lines. Upper panel: cross sections for *e/f* conserving transitions; both the experimental and theoretical values plotted are the average of the $e \rightarrow e$ and $f \rightarrow f$ cross- sections (eq 5a). Lower panel: cross sections for *e/f* changing transitions; both the experimental and theoretical values plotted are the average of the $e \rightarrow f$ and $f \rightarrow e$ cross sections (eq 5b).

observed here: a propensity toward *e/f* conservation for *even* ΔJ and *e/f* reversal for *odd* ΔJ.

We see also that the cross sections determined with the $\langle r \rangle_{20}$ PESs agree better with the experimental results in Figure 9, particularly for transitions with large ΔJ. This is a direct consequence of the increased angular anisotropy in V_{sum}, as compared with the r_e PES. Increased anisotropy will lead to an increasing degree of rotational excitation. This effect is rendered more apparent if we consider the average rotational energy transfer

$$\langle \Delta E_{\text{rot}} \rangle \equiv \frac{\sum_{J'} \sigma_{J \rightarrow J'} (e_{J'} - e_J)}{\sum_{J'} \sigma_{J \rightarrow J'}} \qquad (6)$$

The values of $\langle \Delta E_{\text{rot}} \rangle$ are given in Table 1. We observe a substantial increase in $\langle \Delta E_{\text{rot}} \rangle$, as anticipated, with the $\langle r \rangle_{20}$ PES. However, the experimental value of $\langle \Delta E_{\text{rot}} \rangle$ remains a bit larger. There are several possible explanations for this discrepancy: First, the angular anisotropy may still be underestimated in the $\langle r \rangle_{20}$ PESs, because of contributions from extended values of r near the outer turning point of the NO ($v = 20$) vibrational wave function (Figure 1). We did carry out some preliminary calculations of the PESs for values of r larger than $\langle r \rangle_{20}$. Unfortunately, the convergence difficulties, which are mentioned in section V and are due to configurational mixing with excited electronic states of the NO molecule, become even more pronounced at larger values of r. These could possibly be circumvented by use of a multireference, configuration interaction, rather than CEPA, method. However, the former would be far more computationally intensive.

It is possible although we believe unlikely that the increased degree of rotational excitation in the experimental results may

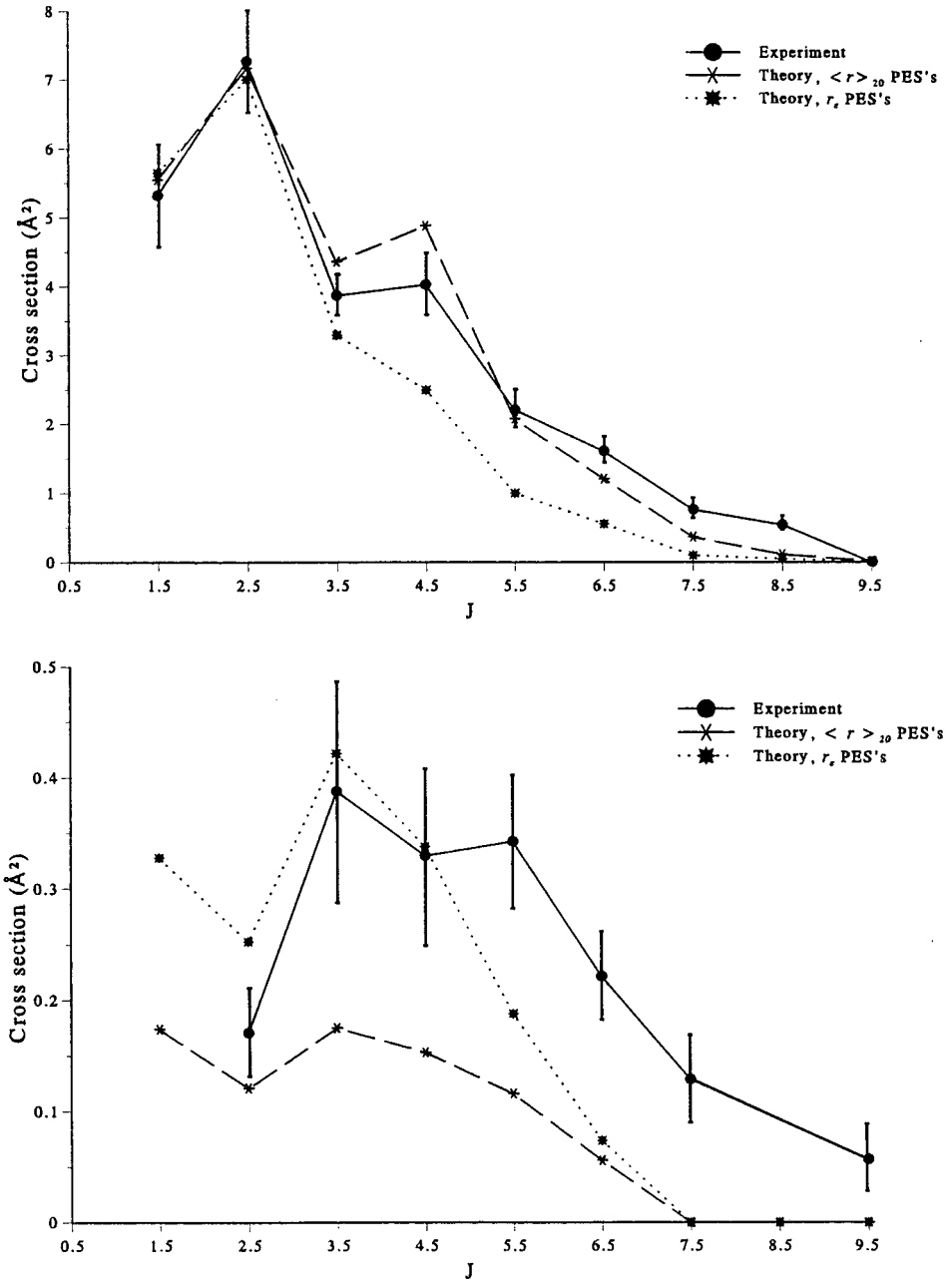

Figure 10. Comparison of the Λ-doublet averaged cross sections for spin−orbit conserving, $\Omega = {}^1/_2 \rightarrow \Omega = {}^3/_2$, transitions (upper panel) and spin−orbit changing, $\Omega = {}^1/_2 \rightarrow \Omega = {}^3/_2$, transitions (lower panel). The values plotted are the summed and averaged cross-sections defined by eq 6. To guide the eye the points have been connected by straight lines.

be due to sampling of collision energies substantially higher than the mean value of 195 cm^{-1}. In that case, one might expect an increased degree of rotational excitation with increasing collision energy. To simulate the effect of the finite distribution of collision energies, we have performed additional scattering calculations at $E = 162$ and 228 and 300 cm^{-1}. The cross sections at these energies, as well as those at $E = 195$ cm^{-1} were averaged over the observed distribution of collision energies (fwhm = 65 cm^{-1}; see the last paragraph in section III). The energy-averaged cross sections, however, differ insignificantly from the values calculated for $E_{col} = 195$ cm^{-1}, as can be seen in Table 1.

We believe it unlikely, but possible, that the small remaining discrepancies between experiment and theory are due to secondary collisions in the crossed molecular beam arrangement. An argument that the differences are real is as follows. Secondary collisions would wash out the amplitude of the even-*J*/odd-*J* oscillations in the rotational dependence of the cross-sections. See for example Figure 9. Specifically, if large observed ΔJ are due to secondary collisions the even−odd amplitude should be less at high *J* than at low *J*. However, this aspect of the observations agrees very well with theory. If anything the theory slightly underestimates the amplitude of this effect for larger ΔJ. Given the substantial improvement in the agreement between theory and experiment by fixing the NO bond length at 2.60 bohr, $\langle r \rangle_{20}$, in comparison to 2.17 bohr, r_e; it is clear that the effect of extending the NO bond length is important to the theoretical calculations of the rotational scattering dynamics. Inspection of Figure 1 reveals that a substantial portion of the NO($v = 20$) wave function extends out much further than 2.6 bohr. Indeed, the last maximum in the $v = 20$ vibrational wave function occurs at $r \approx 3.2$ bohr. Thus a significant fraction of the collisions will sample NO molecules stretched substantially beyond the equilibrium bond length. Therefore, it seems most likely that the small remaining differences between experiment and theory are due to the

TABLE 2: Experimental and Theoretical State-to-State Cross Sections (Å^2) for Spin−Orbit Changing ($\Omega = {}^1/_2 \rightarrow {}^3/_2$) Transitions in Collisions of NO $X\ ^2\Pi_{1/2}$($v = 20$, $J = 0.5$, *e/f* Symmetry) with He at an Average Collision Energy of 195 cm^{-1}

		theory[b]	
J'	exp[a]	r_e PES	$\langle r\rangle_{20}$ PES
1.5	*c*	0.33	0.17
			0.17
2.5	0.17 ± 0.04	0.25	0.12
			0.12
3.5	0.39 ± 0.10	0.42	0.18
			0.17
4.5	0.33 ± 0.08	0.34	0.15
			0.15
5.5	0.34 ± 0.06	0.19	0.12
			0.11
6.5	0.22 ± 0.04	0.07	0.06
7.5	0.13 ± 0.04	*d*	*d*
8.5	*c*	*d*	*d*
9.5	0.05 ± 0.03	*d*	*d*

[a] The absolute magnitude of the experimental cross sections was set by comparison of the final *e/f* unresolved cross sections into $J' = 4.5$ for both spin−orbit changing (this table) and spin−orbit conserving (Table 1) cross sections, with the later value set equal to the experimentally found value ($\sigma = 4.08$ Å^2). The reported values are given within a 95% confidence level. [b] Tabulated here are the summed and averaged cross sections defined by eq 7. The second line in the fourth column corresponds to an average, over the experimental distribution of collision energies, determined using cross sections calculated at $E = 162$, 195, 228, and 300 cm^{-1}. [c] No cross sections could be determined due to spectral overlap. [d] These rotational levels are energetically closed at a collision energy of 195 cm^{-1}.

treatment of NO($v = 20$) as a rigid rotor. A much more important conclusion is that an outstanding level of agreement between experiment and theory is found using a rigid rotor assumption.

As discussed in section IV, the cross sections for the spin−orbit changing ($\Omega = 0.5 \rightarrow 1.5$) transitions are more than an order of magnitude smaller than those for spin−orbit conserving transitions. Consequently, the former were experimentally monitored using the more sensitive $B-X$ transition. Because the resolution of individual Λ-doublet levels of the final state was not possible for this transition (see section IV), no information could be obtained on the *e/f* dependence of these spin−orbit changing cross sections. As a result, we compare the experimentally measured cross sections to the averaged sum of the cross sections into both Λ-doublet levels of the final state, in other words

$$\sigma_{avg} = {}^1/_2[\sigma_{e\rightarrow e} + \sigma_{e\rightarrow f} + \sigma_{f\rightarrow e} + \sigma_{f\rightarrow f}] \qquad (7)$$

To normalize the cross sections for spin−orbit changing collisions relative to those for spin−orbit conserving transitions, which have been previously normalized as described in the preceding paragraph, we used the $B\ ^2\Pi(v = 5)$ state to probe the collision-induced population in the $J = 4.5$ level of both spin−orbit states (again summed over both Λ-doublets). No experimental cross sections could be determined for $J = 1.5$ and $J = 8.5$ rotational levels due to spectral overlap for these transitions. Table 2 and Figure 10 compare the experimental cross sections for spin−orbit changing transitions, normalized as described above, with the theoretical predictions. Examining now the cross sections for spin−orbit changing transitions, we observe first that the theoretical cross-sections determined for the $\langle r\rangle_{20}$ PESs are *smaller* than those for the r_e PES. As discussed in section V, in connection with Figure 8, the difference potential is *smaller* for the former PESs. Consequently, the calculated cross sections for spin−orbit changing transitions, which in the Hund's case (*a*) limit are coupled solely by the difference potential,[5,8] are smaller. The agreement with experiment is less satisfactory than in the case of the spin−orbit conserving transitions. Although the variation of the magnitude of the cross sections with ΔJ is well reproduced in the theoretical simulation, the $\langle r\rangle_{20}$ cross sections themselves are too small, by roughly a factor of 2.

This discrepancy may be caused by errors in the calculated "difference" PES, which is obviously more sensitive to errors in the A' and A'' surfaces than is the "sum" PES. Alternatively imperfections in the experiment may account for these differences. As already mentioned, the collision energy distribution has a fwhm of about 65 cm^{-1}. The high-energy tail of the distribution of collision energies might be particularly important for the spin−orbit changing transitions, which are 114 cm^{-1} more endoergic than the spin−orbit conserving transitions. We notice, in particular, that cross sections are observed into the $J = 9.5$, $\Omega = {}^3/_2$ level, which lies ∼245 cm^{-1} above the initially populated $J = 0.5$, $\Omega = 0.5$ level. Although we have attempted to take this into account in the theoretical calculations by averaging the calculated cross sections over the experimental collision energy distribution, it may be that a stronger collision energy dependence exists in the experiment than we have found in the theory.

VIII. Conclusion

We have used a crossed molecular beam experiment with stimulated emission pumping to determine relative state-to-state cross sections for inelastic scattering of NO($X\ ^2\Pi$, $v = 20$, $J = 0.5$, *e/f*) by He. The cross sections show strong $\Delta J =$ even propensities for the *e/f* symmetry conserving, spin−orbit conserving transitions and a $\Delta J =$ odd propensity for *e/f*-changing, spin−orbit conserving transitions. Quantum scattering calculations are carried out based on a new ab initio NO−He potential energy surface in which the NO bond is fixed at the average bond length of the $v = 20$ vibrational state. These calculations are compared with those based on an earlier PES appropriate to the NO molecule in $v = 0$. The stretched PES has a greater degree of angular anisotropy which causes a larger degree of rotational excitation. The calculated and experimental cross sections for the spin−orbit conserving transitions are in excellent agreement. This is a remarkable result considering that the highly vibrationally excited NO is essentially treated as a rigid rotor. For the spin−orbit changing transitions, which are sensitive primarily to the effect of the orientation of the antibonding π orbital of the NO molecule on the overall interaction potential, the agreement is somewhat less satisfying.

Acknowledgment. M.H.A. and M.Y. wish to acknowledge the support of the National Science Foundation, under Grant CHE-9629385. M.D. and A.M.W. thank the AFOSR under Grant F49620-95-1-0234 as well as the Santa Barbara Laser Pool funded under NSF Grant CHE-9411302.

References and Notes

(1) Castillo, J. F.; Manolopoulos, D. E.; Stark, K.; Werner, H.-J. *J. Chem. Phys.* **1996**, *104*, 6531.
(2) Ruhbahn, H.-G.; Bergmann, K. *Annu. Rev. Phys. Chem.* **1990**, *41*, 735.
(3) Dagdigian, P. J. In *Dynamics and Kinetics of Small Radicals*; Liu, K. Wagner. A. F., Eds.
(4) Dagdigian, P. J. *Adv. Phys. Chem.*, in press.
(5) Alexander, M. H. *J. Chem. Phys.* **1982**, *76*, 5974.
(6) Alexander, M. H.; Orlikowski, T. *J. Chem. Phys.* **1984**, *80*, 1506.
(7) Orlikowski, T.; Alexander, M. H. *J. Chem. Phys.* **1984**, *80*, 4133.
(8) Alexander, M. H. *Chem. Phys.* **1985**, *92*, 337.

(9) Corey, G. C.; Alexander, M. H. *J. Chem. Phys.* **1986**, *85*, 5652.
(10) Dagdigian, P. J.; Alexander, M. H.; Liu, K. *J. Chem. Phys.* **1989**, *91*, 839.
(11) Keil, M.; Slankas, J. T.; Kuppermann, A. *J. Chem. Phys.* **1979**, *70*, 541.
(12) Thuis, H.; Stolte, S.; Reuss, J. *Chem. Phys.* **1979**, *43*, 351.
(13) Thuis, H. H. M.; Stolte, S.; Reuss, J.; van den Biesen, J. J. H.; van den Meijdenberg, C. J. N. *Chem. Phys.* **1980**, *52*, 211.
(14) Kosanetzky, J.; List, U.; Urban, W.; Vormann, H.; Fink, E. H. *Chem. Phys.* **1980**, *50*, 361, and references therein.
(15) Sudbø, A. S.; Loy, M. M. T. *Chem. Phys. Lett.* **1981**, *82*, 135.
(16) Sudbø, A. S.; Loy, M. M. T. *J. Chem. Phys.* **1982**, *76*, 3646.
(17) Andresen, P.; Joswig, H.; Pauly, H.; S. R. *J. Chem. Phys.* **1982**, *77*, 2204.
(18) Casavecchia, P.; Lagana, A.; Volpi, G. G. *Chem. Phys. Lett.* **1984**, *112*, 445.
(19) Wight, C. A.; Donaldson, D. J.; Leone, S. R. *J. Chem. Phys.* **1985**, *83*, 660.
(20) Joswig, H.; Andresen, P.; Schinke, R. *J. Chem. Phys.* **1986**, *84*, 1904.
(21) Jons, S. D.; Shirley, J. E.; Vonk, M. T.; Giese, C. F.; Gentry, W. R. *J. Chem. Phys.* **1992**, *97*, 7831.
(22) Suits, A. G.; Bontuyan, L. S.; Houston, P. L.; Whitaker, B. J. *J. Chem. Phys.* **1992**, *96*, 8618.
(23) Yang, X.; Wodtke, A. M. *J. Chem. Phys.* **1992**, *96*, 5111.
(24) Yang, X.; Wodtke, A. M. *J. Chem. Phys.* **1992**, *96*, 5123.
(25) Meyer, H. *J. Chem. Phys.* **1995**, *102*, 3151.
(26) van Leuken, J. J.; van Amerom, F. H. W.; Bulthuis, J.; Snijders, J. G.; Stolte, S. *J. Phys. Chem.* **1995**, *99*, 15573.
(27) Bieler, C. R.; Sanov, A.; Reisler, H. *Chem. Phys. Lett.* **1995**, *235*, 175.
(28) Islam, M.; Smith, I. W. M.; Wiebracht, J. W. *J. Chem. Phys.* **1995**, *103*, 9676.
(29) van Leuken, J. J.; Bulthuis, J.; Stolte, S.; Snijders, J. G. *Chem. Phys. Lett.* **1996**, *260*, 595.
(30) Jons, S. D.; Shirley, J. E.; Vonk, M. T.; Giese, C. F.; Gentry, W. R. *J. Chem. Phys.* **1996**, *105*, 5397.
(31) Nielson, G. C.; Parker, G. A.; Pack, R. T. *J. Chem. Phys.* **1977**, *66*, 1396.
(32) Orlikowski, T.; Alexander, M. H. *J. Chem. Phys.* **1983**, *79*, 6006.
(33) Alexander, M. H. *J. Chem. Phys.* **1993**, *99*, 7725.
(34) Yang, M.; Alexander, M. H. *J. Chem. Phys.* **1995**, *103*, 6973.
(35) McGuire, P.; Kouri, D. J. *J. Chem. Phys.* **1974**, *60*, 2488.
(36) Kouri, D. J. In *Atom-Molecule Collision Theory: A Guide for the Experimentalist*; Bernstein, R. B., Ed.; Plenum: New York, 1979; p 301.
(37) Bontuyan, L. S.; Suits, A. G.; Houston, P. L.; Whitacker, B. J. *J. Phys. Chem.* **1993**, *97*, 6342.
(38) Meyer, W. *Int. J. Quantum Chem. Symp.* **1971**, *5*, 341.
(39) Meyer, W. *J. Chem. Phys.* **1973**, *58*, 1017.
(40) Meyer, W. *Theor. Chim. Acta* **1974**, *35*, 277.
(41) Brown, J. M.; Hougen, J. T.; Huber, K.-P.; Johns, J. W. C.; Kopp, I.; Lefebvre-Brion, H.; Merer, A. J.; Ramsay, D. A.; Rostas, J.; Zare, R. N. *J. Mol. Spectrosc.* **1975**, *55*, 500.
(42) Geuzenbroek, F. H.; Tenner, M. G.; Kleyn, A. W.; Zacherias, H.; Stolte, S. *Chem. Phys. Lett.* **1991**, *187*, 520.
(43) Hamilton, C. E.; Kinsey, J. L.; Field, R. W. *Annu. Rev. Phys. Chem.* **1986**, *37*, 493.
(44) Yang, X.; Wodtke, A. M. *J. Chem. Phys.* **1990**, *92*, 116.
(45) Yang, X.; Mcquire, D.; Wodtke, A. M. *J. Mol. Spectrosc.* **1992**, *154*, 361.
(46) Ma, Z.; Jons, S. D.; Giese, C. F.; Gentry, W. R. *J. Chem. Phys.* **1991**, *94*, 8608.
(47) Dittmann, P.; Pesl, F. P.; Martin, J.; Coulston, G. W.; He, G. Z.; Bergmann, K. *J. Chem. Phys.* **1992**, *97*, 9472.
(48) Gaubatz, U.; Rudecki, P.; Schiemann, S.; B. K. *J. Chem. Phys.* **1990**, *92*, 5363.
(49) Drabbels, M.; Wodtke, A. M. *J. Chem. Phys.* **1997**, *106*, 3024−28.
(50) Herzberg, G. *Spectra of Diatomic Molecules*, 2nd ed.; Van Nostrand: Princeton, NJ, 1968.
(51) Scoles, G. *Atomic and Molecular Beam Methodes*; Oxford University Press: New York, 1988.
(52) Macdonald, R. G.; Liu, K. *J. Chem. Phys.* **1989**, *91*, 821.
(53) Werner, H.-J.; Follmeg, B.; Alexander, M. H. *J. Chem. Phys.* **1988**, *89*, 3139.
(54) Kendall, R. A.; Dunning, T. H., Jr.; Harrison, R. J. *J. Chem. Phys.* **1992**, *96*, 6796.
(55) Dunning, T. H., Jr., *J. Chem. Phys.* **1989**, *90*, 1007.
(56) MOLPRO is a package of ab initio programs written by H.-J. Werner and P. J. Knowles, with contributions from J. Almlöf, R. D. Amos, M. J. O. Deegan, S. T. Elbert, C. Hampel, W. Meyer, K. Peterson, E. A. Reinsch, R. Pitzer, A. Stone and P. R. Taylor.
(57) Bergmann, K.; Demtröder, W. *Z. Phys.* **1971**, *243*, 1.
(58) Klar, H. *J. Phys. B* **1973**, *6*, 2139.
(59) Green, S.; Zare, R. N. *Chem. Phys.* **1975**, *7*, 62.
(60) Boys, S. F.; Benardi, F. *Mol. Phys.* **1970**, *19*, 553.
(61) Lefebvre-Brion, H.; Field, R. W. *Perturbations in the Spectra of Diatomic Molecules*; Academic: New York, 1986.
(62) Amiot, C. *J. Mol. Spectrosc.* **1982**, *94*, 150.
(63) Arthurs, A.; Dalgarno, A. *Proc. R. Soc. (London Ser.)* **1960**, *A256*, 540.
(64) HIBRIDON is a package of programs for the time-independent quantum treatment of inelastic collisions and photodissociation written by M. H. Alexander, D. E. Manolopoulos, H.-J. Werner, and B. Follmeg, with contributions by P. F. Vohralik, D. Lemoine, G. Corey, B. Johnson, T. Orlikowski, W. Kearney, A. Berning, A. Degli-Esposti, C. Rist, and P. Dagdigian. More information and/or a copy of the code can be obtained at the website http://www-mha.umd.edu/∼mha/hibridon.
(65) Alexander, M. H.; Andresen, P.; Bacis, R.; Bersohn, R.; Comes, F. J.; Dagdigian, P. J.; Dixon, R. N.; Field, R. W.; Flynn, G. W.; Gericke, K.-H.; Grant, E. R.; Howard, B. J.; Huber, J. R.; King, D. S.; Kinsey, J. L.; Kleinermanns, K.; Kuchitsu, K.; Luntz, A. C.; MacCaffery, A. J.; Pouilly, B.; Reisler, H.; Rosenwaks, S.; Rothe, E.; Shapiro, M.; Simons, J. P.; Vasudev, R.; Wiesenfeld, J. R.; Wittig, C.; Zare, R. N. *J. Chem. Phys.* **1988**, *89*, 1749.
(66) Degli Esposti, A.; Berning, A.; Werner, H.-J. *J. Chem. Phys.* **1995**, *103*, 2067.